Three-Dimensional Cone Filter Banks

L. T. Bruton, *Fellow, IEEE*

***Abstract*—Three dimensional (3-D) narrow cone-shaped filter passbands are ideally required for the selective filtering of sampled broad-band 3-D plane waves on the basis of their directions of arrival. A method is proposed for approximating narrow 3-D cone-shaped passbands using a 3-D cone-filter-bank structure in which the subbands consist of band limited 3-D narrow-band infinite impulse response (IIR) beam filters having 3-D uniform bandwidths that are approximately proportional to their distance from the origin in the 3-D frequency space. The 3-D beam filters may be realized from a cascade of 3-D IIR frequency-planar filters. It is shown that the proposed 3-D cone filter bank achieves low distortion of broad-band passband 3-D plane waves, and significant attenuation of broad stopband plane waves.**

***Index Terms*—Three-dimensional (3-D) cone filters.**

I. Introduction

THERE are many applications for discrete-domain filters that selectively filter broad-band three-dimensional (3-D) plane waves (PWs) on the basis of their directions of arrival (DOAs). These applications often involve the selective filtering (or enhancement) of a desired continuous-domain space–time (ST) PW signal, emanating from a distant source and arriving at the receiver as a 3-D PW in superposition with undesirable signals, such as noise and other 3-D PWs, including reflections of the desired PW. Examples of such applications exist in astronomy, wireless communications, sonar imaging, seismic imaging, biomedical imaging, and directional audio systems.

The ideal *continuous-domain* 3-D PW signal $x_{\mathrm{PWC}}(\mathbf{t})$, $\mathbf{t} \in \mathbb{R}^3$, may be written in the form

$$x_{\mathrm{PWC}}(\mathbf{t}) = x(l) \qquad \forall\, l \in \mathbb{R}^1 | \mathbf{d}_{\mathbf{D}}^{\mathbf{T}}\,\mathbf{t} = l \tag{1.1}$$

where $\mathbf{d}_{\mathbf{D}}$ is the unit vector in the DOA and $x(l)$ is a one-dimensional (1-D) function describing the intensity of the signal in the DOA.

The region of support (ROS) of the 3-D Fourier magnitude spectrum $|X_{\mathrm{PWC}}(j\boldsymbol{\omega})|$ of $x_{\mathrm{PWC}}(\mathbf{t})$ lies on the straight line in $\boldsymbol{\omega} \in \mathbb{R}^3$ that passes through the origin $\boldsymbol{\omega} = 0$ and is oriented in direction $\mathbf{d}_{\mathbf{D}}^{\mathbf{T}}$ [1]. An ideal continuous-domain 3-D PW is considered to be *broad-band* if the ROS of $|X_{\mathrm{PWC}}(j\boldsymbol{\omega})|$ is broadly distributed along this line; that is, not localized to a narrow part of the line. If a 3-D filter is required to selectively transmit 3-D broad-band PWs having DOAs that are restricted to lie within a small angle ε of $\mathbf{d}_{\mathbf{D}}^{\mathbf{T}}$ of $x_{\mathrm{PWC}}(\mathbf{t})$, then the 3-D passband must ideally be the 3-D cone in $\boldsymbol{\omega} \in \mathbb{R}^3$ having its vertex at the origin in $\boldsymbol{\omega}$ and its axis in the direction $\mathbf{d}_{\mathbf{D}}$ [2], as shown in Fig. 1. The *ideal* continuous-domain 3-D magnitude frequency response $|H_{\mathrm{CONE}}(j\boldsymbol{\omega})|$ of this 3-D cone filter is defined to equal unity inside the passband of the cone, and zero elsewhere in $\boldsymbol{\omega} \in \mathbb{R}^3$.

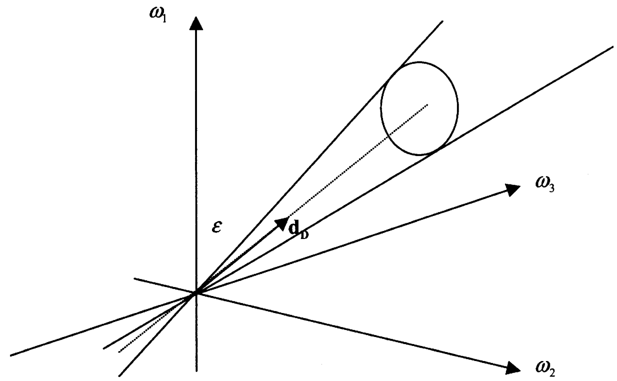

Fig. 1. Ideal continuous-domain 3-D cone passband.

We are concerned here with *discrete-domain* methods: that is, methods in which $x_{\mathrm{PWC}}(\mathbf{t})$ is spatio–temporally sampled in 3-D to obtain the corresponding discrete-domain signal $x_{\mathrm{PW}}(n_1, n_2, n_3), \mathbf{n} = [n_1, n_2, n_3] \in \mathbb{N}^3$. In general, the ROS of the spectrum $|X_{\mathrm{PW}}(j\boldsymbol{\omega})|$ of a sampled PW $x_{\mathrm{PW}}(n_1, n_2, n_3)$ is not constrained to lie on the above-mentioned 3-D line due to the 3-D periodicity of $|X_{\mathrm{PW}}(j\boldsymbol{\omega})|$ in $\boldsymbol{\omega}$, the inevitable finite ROS of the sampled signal and possibly due to aliasing.

In order to successfully recover a 3-D PW using discrete-domain 3-D cone filters, it is especially important to avoid significant aliasing. If $|X_{\mathrm{PWC}}(j\boldsymbol{\omega})|$ is nonzero outside of the 3-D Nyquist box (i.e., outside the region $-\pi < \omega_1 \leq \pi$ or $-\pi < \omega_2 \leq \pi$ or $-\pi < \omega_3 \leq \pi$), suitable anti-aliasing filters may be required prior to 3-D sampling and 3-D filtering. In the following, we assume that the Nyquist condition $(|X_{\mathrm{PWC}}(j\boldsymbol{\omega})| = 0\ \forall\, |\omega_{1,2,3}| \geq \pi)$ is met prior to sampling the 3-D PW, implying that the 3-D spectrum of the sampled signal $x_{\mathrm{PW}}(n_1, n_2, n_3)$ has a ROS in $\boldsymbol{\omega} \in \mathbb{R}^3$ that is 3-D periodic and, in each replicated period, has its ROS in the direction of the above-mentioned 3-D line for all $\mathbf{d}_{\mathbf{D}}$.

The 3-D magnitude frequency response $|T_{\mathrm{CONE}}(e^{j\boldsymbol{\omega}})|$ of a corresponding *discrete-domain* 3-D Cone filter should approximate the ideal continuous-domain cone response $|H_{\mathrm{CONE}}(j\boldsymbol{\omega})|$ *inside the 3-D Nyquist box*. However, $|T_{\mathrm{CONE}}(e^{j\boldsymbol{\omega}})|$ is also 3-D-periodic with periodicity 2π in all three frequency variables $\omega_{1,2,3}$. Clearly, if we strived to achieve $|T_{\mathrm{CONE}}(e^{j\boldsymbol{\omega}})| \approx |H_{\mathrm{CONE}}(j\boldsymbol{\omega})|$ everywhere inside the Nyquist box then, for *off-axis* cones, $|T_{\mathrm{CONE}}(e^{j\boldsymbol{\omega}})|$ would possess surface discontinuities where its ROS intersects the surfaces

Manuscript received January 16, 2002; revised July 3, 2002. This work was supported by the Natural Sciences and Engineering Research Council of Canada. This paper was recommended by Associate Editor A. B. da Silva Eduardo.

The author is with the Department of Electrical and Computer Engineering, University of Calgary, Calgary, AB T2N IN4, Canada.

Digital Object Identifier 10.1109/TCSI.2002.808200

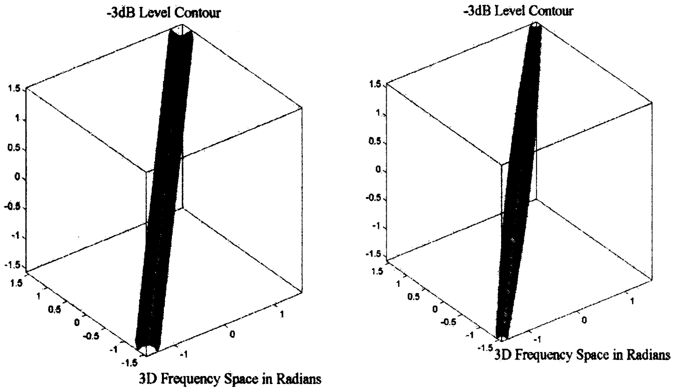

(a) (b)

Fig. 2. Highly directional beam filter, -3-dB level contours of continuous-domain $|H_{\mathrm{BM}}(j\boldsymbol{\omega})|$ and discrete-domain $|T_{\mathrm{BM,\,k}}(e^{j\boldsymbol{\omega}})|$ magnitude frequency responses in the 3-D radian frequency box $-\pi/2 < \omega_i \leq \pi/2,\ i = 1,\ 2,\ 3$.

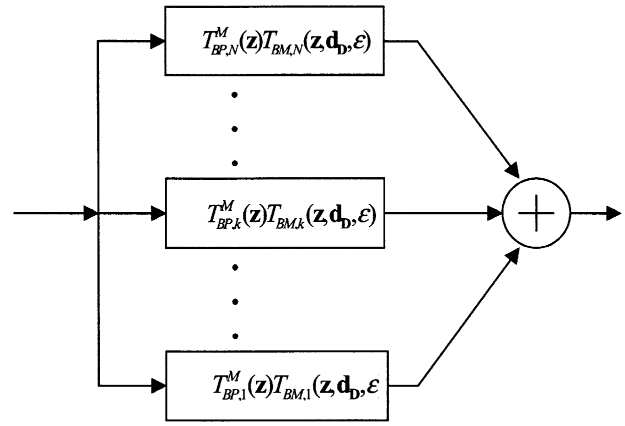

Fig. 3. The 3-D cone filter bank.

of the Nyquist box. Approximating such 3-D discontinuities near the surfaces of the Nyquist box would require very high order 3-D difference equations and considerable computational complexity. It is therefore advisable, for off-axis cones, to place a practical upper limit on the portion of the Nyquist box over which the approximation $|T_{\mathrm{CONE}}(e^{j\boldsymbol{\omega}})| \approx |H_{\mathrm{CONE}}(j\boldsymbol{\omega})|$ is to be accurately achieved. [An analogous 1-D problem occurs, where $|\omega_1| = \pi$, in the approximation of ideal 1-D differentiators $H(j\omega_1) = j\omega_1$.]

Most previously reported approaches to the 3-D cone filter design problem fall into one of several broad categories. First, algebraically-designed recursive discrete-time *3-D IIR beam filters* have been proposed [1] which yield narrow beam angles (that is, high directional selectivity in ST) and low computational complexity. A typical continuous-domain recursive beam filter magnitude response $|H_{\mathrm{BM}}(j\boldsymbol{\omega})|$ is illustrated by the -3-dB gain level contour, $|H_{\mathrm{BM}}(j\boldsymbol{\omega})| = 1/\sqrt{2}$, shown in Fig. 2(a). For the purpose of filtering sampled PWs, such beam filters achieve rather poor approximation to a 3-D cone passband, although they have been used to selectively filter sampled 3-D PWs. For the purpose of filtering broad-band sampled PWs, the *uniform* 3-D bandwidth of a beam shaped passband causes excessive frequency selectivity at high frequencies and insufficient frequency selectivity at low frequencies.

A second set of methods for designing 3-D cone filters employs *numerical approximation* techniques. For example, it is shown in [1] that two-dimensional (2–D) IIR fan filter prototype transfer functions may be employed to realize stable rotated 3-D wedge-shaped passbands and that, by cascading such wedge-shaped passband transfer functions, it is possible to make a good approximation to 3-D cone-shaped passbands. The implementation of the wedge-shaped functions is achieved by numerical optimization. It has also been proposed [4] that 3-D cone filters be designed directly by numerical optimization, starting with an algebraic expression for the cone function and using the 3-D discrete Fourier transfor (DFT) to calculate the transfer function at discrete 3-D frequencies. Again, the reported methodology relies on numerical optimization and it is necessary to repeat the optimization for each different required combination of cone width ε and cone direction $\mathbf{d_D}$.

An *algebraic filter bank method* is proposed here [8] that yields closed form approximations for the 3-D recursive discrete-domain cone filter Z-transform transfer function $T_{\mathrm{CONE}}(\mathbf{z},\ \mathbf{d_D},\ \varepsilon)$ *as a function of the DOA* $\mathbf{d_D}$ *and cone angle* ε. The 3-D steady-state frequency response transfer function $|T_{\mathrm{CONE}}(e^{j\boldsymbol{\omega}},\ \mathbf{d_D},\ \varepsilon)|$ and the 3-D input–output difference equation may be obtained directly (and algebraically) from $T_{\mathrm{CONE}}(\mathbf{z},\ \mathbf{d_D},\ \varepsilon)$ in terms of the prescribed design parameters $\mathbf{d_D}$ and ε. The resultant 3-D IIR cone filter has a cone-shaped passband and lower computational complexity than comparable 3-D FIR methods. It is shown that passband PWs may be selectively filtered with low distortion in the region of ST where the ST transient response has decayed sufficiently. For ST applications, where one of the components of $\mathbf{t} = (t_1,\ t_2,\ t_3)$ is time, the algebraic representation for $T_{\mathrm{CONE}}(\mathbf{z},\ \mathbf{d_D},\ \varepsilon)$ allows $\mathbf{d_D}$ and ε to be adapted in ST to track incoming PWs on the basis of their DOAs.

II. 3-D Cone Filter Bank

The structure of the proposed discrete-domain filter bank, referred to as the 3-D cone filter bank, is shown in Fig. 3. It consists of N bands, where each subband k is composed of a 3-D IIR frequency-beam filter $T_{\mathrm{BM,\,k}}(\mathbf{z},\ \mathbf{d_D},\ \varepsilon)$ in cascade with a 3-D band pass filter $T^{M}_{\mathrm{BP,\,k}}(\mathbf{z})$ of order M. The notation $T_{\mathrm{BM,\,k}}(\mathbf{z},\ \mathbf{d_D},\ \varepsilon)$ implies that the kth Z transform transfer function of the subband beam filter is determined by the prescribed cone design parameters $\mathbf{d_D}$ and ε whereas the subband bandpass filters $T^{M}_{\mathrm{BP,\,k}}(\mathbf{z})$ are designed independently of these parameters. It is shown here that the N bandpass filters $T^{M}_{\mathrm{BP,\,k}}(\mathbf{z})$, $k = 1,\ 2,\ \ldots N$, may be implemented as 1-D filters and the 3-D IIR frequency-beam filters $T_{\mathrm{BM,\,k}}(\mathbf{z},\ \mathbf{d_D},\ \varepsilon)$ as a cascade $T_{\mathrm{FP1}}(\mathbf{z},\ \mathbf{d_1},\ \varepsilon)T_{\mathrm{FP2}}(\mathbf{z},\ \mathbf{d_2},\ \varepsilon)$ of two 3-D IIR frequency-planar filters where $\mathbf{d_1}$ and $\mathbf{d_2}$ are the normals to the frequency planes of $T_{\mathrm{FP1}}(\mathbf{z},\ \mathbf{d_1},\ \varepsilon)$ and $T_{\mathrm{FP2}}(\mathbf{z},\ \mathbf{d_2},\ \varepsilon)$. It follows from Fig. 3 that the transfer function of the 3-D cone filter bank is given by

$$T_{\mathrm{CONE}}(\mathbf{z},\ \mathbf{d_D},\ \varepsilon) = \sum_{k=1}^{N} T^{M}_{\mathrm{BP,\,k}}(\mathbf{z})T_{\mathrm{BM,\,k}}(\mathbf{z},\ \mathbf{d_D},\ \varepsilon). \quad (2.1)$$

III. Review: Implementing 3-D Beam Filters by Cascading 3-D Frequency-Planar Filters

The design of highly directional 3-D recursive beam filters is briefly reviewed here. In [1], 3-D recursive frequency-beam filters are implemented using a cascade of two 3-D Practical-BIBO stable [3] frequency-planar recursive filters $H_{\mathrm{FP1}}(\mathbf{s})$ and $H_{\mathrm{FP2}}(\mathbf{s})$ to yield the continuous-domain 3-D beam-frequency Laplace transform transfer function

$$\begin{aligned} H_{\mathrm{BM}}(\mathbf{s}) &\equiv H_{\mathrm{FP1}}(\mathbf{s})H_{\mathrm{FP2}}(\mathbf{s}) \\ &= \left(\frac{1}{1+\frac{1}{B_1}\mathbf{d_1^T s}}\right)\left(\frac{1}{1+\frac{1}{B_2}\mathbf{d_2^T s}}\right) \end{aligned} \tag{3.1}$$

where $\mathbf{d_{1,\,2}}$ are unit vectors normal to the respective frequency passband planes of $H_{\mathrm{FP1,\,FP2}}(\mathbf{s})$ and $B_{1,\,2}$ are the -3-dB bandwidths of the frequency-planar filters. The functions $H_{\mathrm{FP1,\,FP2}}(\mathbf{s})$ have 3-D magnitude frequency response transfer functions $|H_{\mathrm{FP1,\,FP2}}(j\boldsymbol{\omega})|$ that, for $B_{1,\,2} \ll 1$, closely surround the 3-D planes

$$\mathbf{d_1^T}\boldsymbol{\omega} = 0 \quad \text{and} \quad \mathbf{d_2^T}\boldsymbol{\omega} = 0 \tag{3.2}$$

respectively. The four -3-dB planes (that is, -3-dB level contours) $P_1^{\pm}$ and $P_2^{\pm}$ are given by

$$P_1^{\pm} \equiv \boldsymbol{\omega} \in \mathbb{R}^3 | \mathbf{d_1^T}\boldsymbol{\omega} = \pm\frac{1}{B_1}$$

and

$$P_2^{\pm} \equiv \boldsymbol{\omega} \in \mathbb{R}^3 | \mathbf{d_2^T}\boldsymbol{\omega} = \pm\frac{1}{B_2}. \tag{3.3}$$

These planes characterize the cross-sectional shapes of the passbands of the two 3-D beam filters. The 3-D frequency-planar transfer functions $H_{\mathrm{FP1,\,FP2}}(\mathbf{s})$ correspond to transfer functions of continuous-domain 3-D resistively-terminated reactance 2 ports [1], for which it has been shown [3] that the 3-D triple bilinear transformation

$$s_i = \frac{z_i - 1}{z_i + 1}, \qquad i = 1,\,2,\,3 \tag{3.4}$$

yields computable Practical-BIBO stable [3] 3-D recursive input–output difference equations in the 3-D discrete domain.

Remark About BIBO Stability and Practical-BIBO Stability: It may easily be shown that application of the triple bilinear transform of (3.4) to (3.1) leads to a 3-D $\mathbf{z}$-domain transfer function having a nonessential singularity of the second kind on the unit polydisc, at $\mathbf{z} = (-1,\,-1,\,-1)$, implying that the resultant 3-D discrete-domain transfer function may be BIBO unstable [9], [10]. However, the 3-D $\mathbf{z}$-domain transfer function *is* Practical-BIBO stable, where Practical-BIBO stability implies that, for all 3-D *spatially-bounded* amplitude-bounded input sequences and all spatially-bounded output sequences, the output sequence is amplitude-bounded [3]. This implication holds for the case of temporally-unbounded spatially-bounded input and output sequences.

With $\mathbf{d_1} \neq \mathbf{d_2}$, the frequency planes in equation (3.2) *intersect in a straight line that passes through the origin* in $\boldsymbol{\omega}$. This line is the passband center line CL of the passband of the beam filter $H_{\mathrm{BM}}(\mathbf{s})$ and is therefore given by

$$CL \equiv \{\boldsymbol{\omega} \in \mathbb{R}^3 | \mathbf{d_1^T}\boldsymbol{\omega} = \mathbf{d_2}^T\boldsymbol{\omega} = 0\}. \tag{3.5}$$

This center line becomes the axis of the cone passband of the proposed 3-D cone filter bank in direction $\mathbf{d_D^T}$.

It follows from (3.1) that $|H_{\mathrm{BM}}(j\boldsymbol{\omega})| = 1$ everywhere on line CL. With $B_{1,\,2} \ll 1$, the 3-D beam passband of $|H_{\mathrm{BM}}(j\boldsymbol{\omega})| = 1$ closely surrounds line CL and has a *constant* cross-sectional 3-D bandwidth. Such 3-D frequency beam filters are highly directional and may be used to selectively filter 3-D PWs having DOA $\mathbf{d_D^T}$ [2]. However, the beam-shaped passband is generally less suitable than a 3-D cone-shaped passband. This is because the constant cross-sectional bandwidth of the beam-shaped passband implies an *angular* selectivity that increases in proportion to distance from the origin in $\boldsymbol{\omega}$ and the passband has relatively poor 3-D selectivity in the low-frequency portion of the spectrum. By definition, a 3-D cone-shaped passband has *constant angular selectivity* and therefore ideally has unity gain for all DOAs within angle ε of $\mathbf{d_D^T}$.

Substituting (3.4) into (3.1), using subscript k for the kth subband and evaluating at $z_{1,\,2,\,3} = \exp(j\omega_{1,\,2,\,3})$, yields the 3-D discrete-domain beam filter frequency response transfer function of band k in the form

$$\begin{aligned} T_{\mathrm{BM,\,k}}(e^{j\boldsymbol{\omega}}) &\equiv \left. H_{\mathrm{BM,\,k}}(\mathbf{s})\right|_{\mathbf{s}=(\boldsymbol{z}-1)/(\boldsymbol{z}+1)|_{\boldsymbol{z}=\exp(j\boldsymbol{\omega})}} \\ &= T_{\mathrm{FP1,\,k}}(e^{j\boldsymbol{\omega}})T_{\mathrm{FP2,\,k}}(e^{j\boldsymbol{\omega}}) \\ &= \left(\frac{1}{1+j\frac{1}{B_{1,k}}\mathbf{d_1^T}\boldsymbol{\Omega}}\right)\left(\frac{1}{1+j\frac{1}{B_{2,k}}\mathbf{d_2^T}\boldsymbol{\Omega}}\right) \end{aligned} \tag{3.6}$$

where

$$\boldsymbol{\Omega} = [2\tan(\omega_1/2) \quad 2\tan(\omega_2/2) \quad 2\tan(\omega_3/2)].$$

The -3-dB contour of the *continuous-domain* beam magnitude transfer function $|H_{\mathrm{BM}}(j\boldsymbol{\omega})|$ in equation (3.1) is shown in Fig. 2(a) for $B_1 = B_2 = 1/5$, $\mathbf{d_1} = [1/\sqrt{2} \;\; -1/\sqrt{2} \;\; 0]^{\mathbf{T}}$, $\mathbf{d_2} = [1/\sqrt{6} \;\; -1/\sqrt{6} \;\; -\sqrt{2/3}]^{\mathbf{T}}$. The direction of the axis of the beam $\mathbf{d_D}$ is normal to the plane containing $\mathbf{d_1}$ and $\mathbf{d_2}$ and is given by $\mathbf{d_D} = [1/\sqrt{3} \;\; 1/\sqrt{3} \;\; 1/\sqrt{3}]^{\mathbf{T}}$. The corresponding -3-dB contour of the *discrete-domain* magnitude transfer function $|T_{\mathrm{BM,\,k}}(e^{j\boldsymbol{\omega}})|$ in (3.6) is shown in Fig. 2(b) with $B_{1,\,k} = B_{2,\,k} = 1/5$.

It is important to recognize that the beam-shaped passbands of $|T_{\mathrm{BM,\,k}}(e^{j\boldsymbol{\omega}})|$ are distorted, relative to $|H_{\mathrm{BM,\,k}}(j\boldsymbol{\omega})|$, by the triple bilinear transformation and this distortion is greatest in the regions $\pi/2 < |\omega_{1,\,2,\,3}| < \pi$. This transformation results in a "pinched-in" warped narrow passband that departs from the ideal beam response but at least has the advantage of avoiding the previously mentioned discontinuities at the edge of the Nyquist box.

IV. Determination of Bandwidths B_{1k} and B_{2k} of Subband Beam Filters

It is a key step in this method to *select the 3-D bandwidths* B_{1k} and B_{2k} *of the* k*th subband beam filters to be approximately proportional to the frequency distance of the* k*th band from the origin in frequency space*. For example, this may be accomplished by selecting the bandwidths of the frequency-planar filters in the kth subbands, $k = 1, 2, \ldots, N$, as follows, for N even

$$B_{1k,\,2k} \equiv \begin{cases} k\,\dfrac{\pi\tan(\varepsilon)}{N}, & k = 1, 2, \ldots, \left(\dfrac{N}{2}+1\right) \\ (N-k+2)\,\dfrac{\pi\tan(\varepsilon)}{N}, & k = \left(\dfrac{N}{2}+2\right), \left(\dfrac{N}{2}+3\right), \ldots, N. \end{cases} \tag{4.1}$$

Other similar expressions can be employed to approximate a cone-shaped passband, provided that the above-mentioned proportionality is approximately maintained. Substituting (4.1) into (3.6) for the beam filter in the kth band and then into equation (2.1) gives the corresponding discrete-domain 3-D frequency response transfer function of the cone filter bank

$$T_{\text{CONE}}(e^{j\boldsymbol{\omega}}) = \sum_{k=0}^{N-1} \frac{T_{\text{BP,k}}^{M}(e^{j\boldsymbol{\omega}})}{\left(1 + j\frac{1}{B_{1k}}\mathbf{d}_1^{\mathbf{T}}\boldsymbol{\Omega}\right)\left(1 + j\frac{1}{B_{2k}}\mathbf{d}_2^{\mathbf{T}}\boldsymbol{\Omega}\right)}. \tag{4.2}$$

V. Realization and Design of Bandpass Subband Filters $T_{\text{BP, k}}^{M}(\mathbf{z})$

The primary function of the bandpass functions $T_{\text{BP, k}}^{M}(e^{j\boldsymbol{\omega}})$ in (4.2) is to *band limit the 3-D beam-shaped passband to a finite ROS on the passband line* CL. Clearly, a *3-D* bandpass filter could be designed to meet this requirement. However, the passbands of *highly directional* cones ($\varepsilon \ll \pi$) have a ROS that very closely surrounds CL, thereby allowing the ROS on the line to be band limited in each band by means of a *1-D* band pass filter, designed such that its upper and lower stopband frequencies appropriately intersect CL, as shown in Fig. 4 for the 2-D case and for $N = 8$ complex bands.

The transfer functions $T_{\text{BP, k}}^{M}(\mathbf{z})$ should *band limit the beam passbands in such a way that the summed outputs of the bands, according to equation* (2.1), *do indeed approximate the required cone-shaped passband*. This is achieved as follows.

A. Delayed Perfect Reconstruction on the n_3 Axis

A number of different types of 1-D filter banks achieve good cone-shaped approximations. Here, it is shown that delayed perfect reconstruction (PR) 1-D symmetric finite impulse response (FIR) N-band filters [7] provide good cone-reconstruction properties with exact PR on the n_3 axis.

Review of 1-D Delayed-PR 1-D FIR Filter Banks: The length-M [i.e., order $(M-1)$] FIR unit impulse responses $h_{\text{BP, k}}^{M}(n_3)$ of the 1-D kth-band bandpass filters $T_{\text{BP, k}}^{M}(\mathbf{z})$ may be realized from the unit impulse response $h_{\text{NB}}^{M}(n_3)$ of

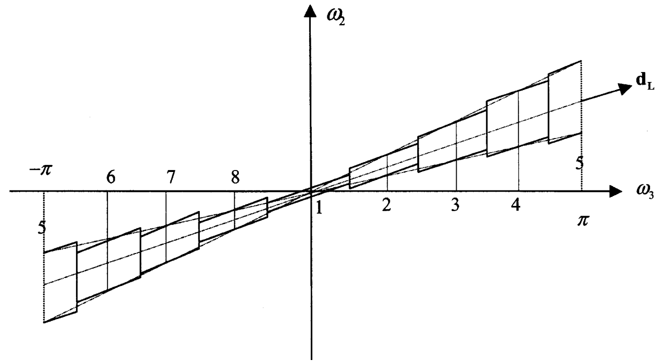

Fig. 4. The 2-D version of the ideal regions of support for the eight complex bands of an 8-band cone filter bank over the full Nyquist interval $-\pi < \omega_3 \leq \pi$.

a *prototype* low pass N-band [7] 1-D FIR filter in which the impulse responses of the bands are given by

$$h_{\text{BP, k}}^{M}(n_3) = h_{\text{NB}}^{M}(n_3).W_N^{-(k-1)n_3}, \qquad k = 1, 2, \ldots, N \tag{5.1}$$

where $W_N \equiv \exp(-j2\pi/N)$ and where the prototype unit impulse response is constrained at every N samples within its ROS as follows:

$$h_{\text{NB}}^{M}(n_3) \equiv \begin{cases} 1/N, & n_3 = r_0 N, \quad r_0 \in \mathbb{N}, \text{constant} \\ 0, & n_3 = rN, \quad r \in \mathbb{N} | r \neq r_0. \end{cases} \tag{5.2}$$

It may be shown that such 1-D filter banks [7] have the overall impulse response

$$\begin{aligned} h(n_3) &= \sum_{k=1}^{N} h_{\text{BP, k}}^{M}(n_3) = \sum_{k=1}^{N} h_{\text{NB}}^{M}(n_3) W_N^{-(k-1)n_3} \\ &= \delta(n_3 - r_0 N) \end{aligned} \tag{5.3}$$

corresponding to delayed PR (i.e., with delay $r_0 N$).

There are many design techniques [7] for obtaining the above N-band low-pass prototype filter $h_{\text{NB}}^{M}(n_3)$. For example, for odd length M, the low-pass N-band impulse response

$$h_{\text{NB}}^{M}(n_3) = \frac{1}{N}\, w(n_3) \text{sinc}\left(\pi\left(n_3 - \frac{M-1}{2}\right)N\right), \quad n_3 = 0, 1, 2, 3, \ldots, (M-1), \quad \frac{M}{N} \notin \mathbb{N}/\{0\} \tag{5.4}$$

satisfies equation (5.2), with $r_0 N = (m-1)/2$. The smoothness of the transitions between bands is improved by choosing the window function $w(n_3)$ as a Hanning window of length M having symmetry about $(M-1)/2$. The 1-D bandpass filters in equation (5.1) have uniform bandwidths $2\pi/N$ spaced uniformly over the frequency interval $-\pi < \omega_3 \leq \pi$.

The steady-state frequency responses of the N bandpass filters are given by

$$\begin{aligned} T_{\text{BP, k}}^{M}(e^{j\boldsymbol{\omega}}) &= Z[h_{\text{BP, k}}^{M}(n_3)]|_{z_3 = e^{j\omega_3}} \\ &= \sum_{n_3=0}^{M-1} h_{\text{BP, k}}^{M}(n_3) e^{-j\omega_3 n_3}, \\ & k = 0, 1, 2, \ldots, (N-1). \end{aligned} \tag{5.5}$$

1) Implementation Using Real Subband Filters: For an even number of bands N, the bandpass impulse responses $h^M_{\mathrm{BP,\,k}}(n_3)$ in (5.3) are real-valued for the two bands 1 and $(N/2)+1$ and complex-valued for the remaining bands $k = 2, 3, \ldots, (N/2), (N/2+2), \ldots, N$, occurring in $(N/2)-1$ conjugate pairs. Each of these conjugate pairs of bands in the 3-D cone filter bank may be combined [7] in order to permit implementation as a *real* NR-band 3-D cone filter bank, where $NR = (N/2)+1$. For example, with $N = 16$, bands 1 and 9 in (5.3) are real valued and bands 2, 3, …, 8 and 10, 11, …, 16 in (5.3) are comples valued, allowing the seven pairs of bands (2, 16), (3, 15), …, (8, 10) to be combined to form seven real bands, resulting in a 9-band (i.e., $NR = 9$) real 3-D cone filter bank.

Although delayed PR is exactly achieved in the direction n_3, the 3-D cone filter bank cannot achieve PR along the other two axes because the 3-D passband is band limited in those directions.

Substituting (5.5) into (4.2) gives the final expression for the 3-D frequency response of the N-band 3-D cone filter bank

$$T_{\mathrm{CONE}}(e^{j\boldsymbol{\omega}}) = \sum_{k=0}^{N-1} \frac{\sum\limits_{n_3=0}^{M-1} h^M_{\mathrm{BP\,k}}(n_3)\exp(-j\omega_3 n_3)}{\left(1+j\frac{1}{B_{k1}}\mathbf{d_1^T\Omega}\right)\left(1+j\frac{1}{B_{k2}}\mathbf{d_2^T\Omega}\right)} \tag{5.6}$$

where $h^M_{\mathrm{BP,\,k}}(n_3)$ is given in (5.1) and (5.4) and $\mathbf{\Omega}$ in (3.6).

The input–output 3-D difference equation is obtained directly from equation (2.1), has input–output masks in each subband of size (2, 2, M+ 2) in the respective three directions of recursion n_1, n_2 and n_3, is IIR in directions n_1 and n_2 and FIR in direction n_3.

VI. 3-D Cone Filter Bank Case Studies

In the following examples, highly directional 3-D cone filter banks are realized using bandpass FIR filters of order 32 in 3-D cone filter banks having nine real bands.

Case 1: Cone Center Line Along the Temporal Axis: Consider the design of a narrow-band cone filter according to equation (4.2) with the following design specification:

$$\mathbf{d_D} \equiv [0 \quad 0 \quad 1]^{\mathbf{T}}, \qquad \varepsilon = 20^o \tag{6.1}$$

over the full Nyquist frequency interval $-\pi < \omega_3 \leq \pi$. This specified value of $\mathbf{d_D}$ points the axis of the cone along the temporal frequency axis ω_3, corresponding to a DOA that is in the direction of the time axis.

The planes of the two beam filters in (3.2) intersect in the cone center line *CL* and must have the direction $\mathbf{d_D}$ prescribed by equation (6.1). There is considerable design flexibility concerning the selection of the normals $\mathbf{d_{1\,2}}$ of the frequency planes of $|H_{\mathrm{FP1,\,FP2}}(j\boldsymbol{\omega})|$. (This is because there are an infinite number of pairs of planes that intersect in a given straight line.) Quadrature unit vectors $\mathbf{d_1} \equiv [1 \quad 0 \quad 0]^{\mathbf{T}}$ and $\mathbf{d_2} \equiv [0 \quad 1 \quad 0]^{\mathbf{T}}$ are selected here and are normals to the frequency-planes $\omega_1 = 0$ and $\omega_2 = 0$ of $H_{\mathrm{FP1}}(\mathbf{s})$ and $H_{\mathrm{FP2}}(\mathbf{s})$, respectively. The line of intersection CL of these two planes is where $\omega_1 = \omega_2 = 0$; this is the required center line in the direction $\mathbf{d_D}$.

The total number of bands in the 3-D Nyquist box is selected as $N = 16$ in order to achieve a total of nine real bands. The

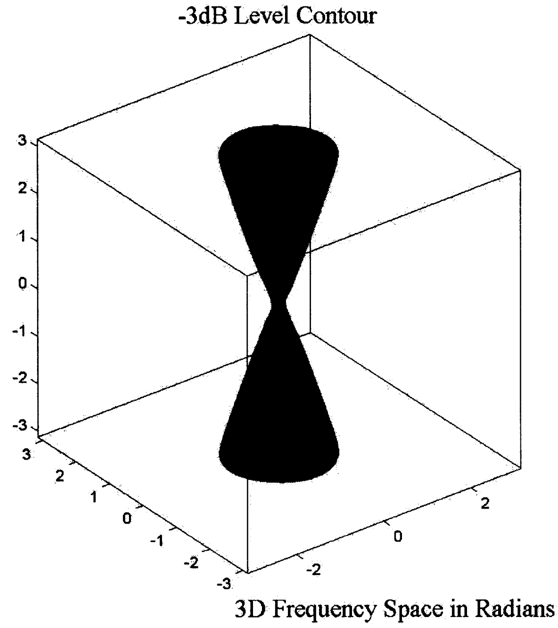

Fig. 5. Case 1: -3-dB level contour of the nine real-band cone filter. $\varepsilon \equiv 20^\circ$. $\mathbf{d_D^T} \equiv [0\ 0\ 1]^{\mathbf{T}}$. Frequencies shown in radians.

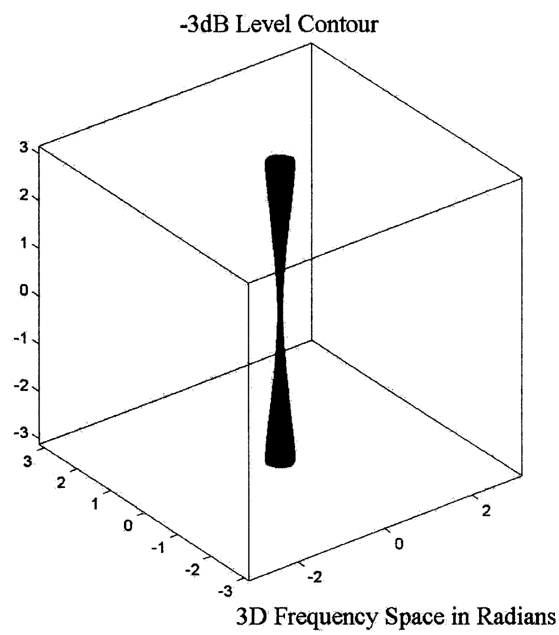

Fig. 6. Case 2: -3-dB level contours of the nine real-band cone filter. $\varepsilon \equiv 5^o$. $\mathbf{d_D^T} \equiv [0 \quad 0 \quad 1]^{\mathbf{T}}$. Frequencies shown in radians.

coefficients $h^M_{\mathrm{NB,\,k}}(n_3)$ of the prototype low-pass N-band FIR filter of length $M = 33$ are given by (5.4) and the length-33 Hanning window $w(n_3)$. Evaluating (5.6) yields the frequency response transfer function $T_{\mathrm{CONE}}(e^{j\boldsymbol{\omega}})$ of the 3-D cone filter bank. As expected, the magnitude frequency transfer response $|T_{\mathrm{CONE}}(e^{j\omega})|$ is exactly unity along the axis of the cone. The -3-dB level surface of $|T_{\mathrm{CONE}}(e^{j\boldsymbol{\omega}})|$ very closely approximates the required cone-shaped passband, as shown in Fig. 5. The phase frequency response transfer function $\angle T_{\mathrm{CONE}}(e^{j\boldsymbol{\omega}})$ is linear and in direction n_3, corresponding in slope to a delay of exactly $n_3 = 16$ in this direction.

Case 2: Variation of the Angular Selectivity of the Cone: The -3 dB level contour of $|T_{\mathrm{CONE}}(e^{j\boldsymbol{\omega}})|$ is shown in Fig. 6 for the

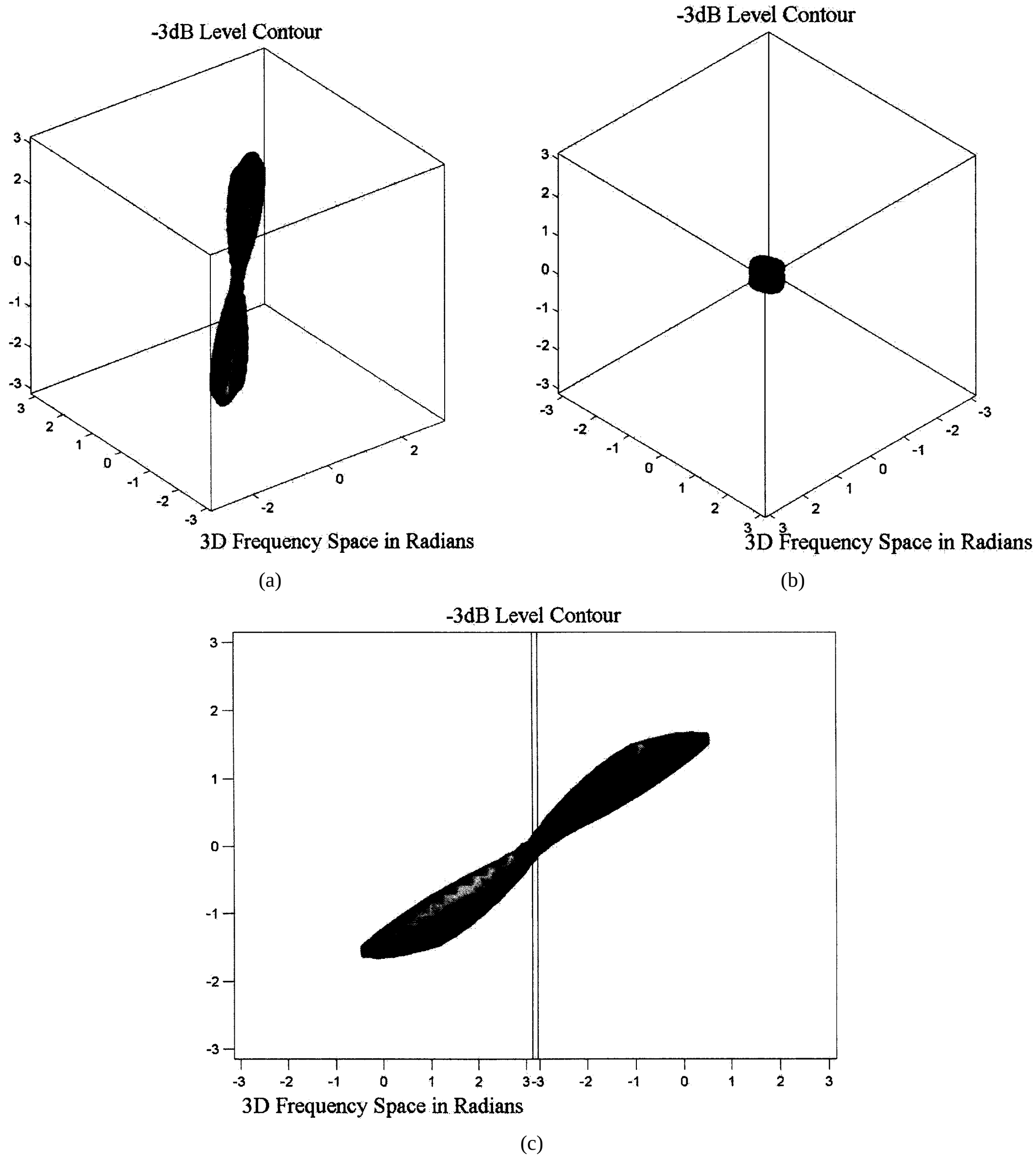

Fig. 7. Case 3: Three views of the -3-dB level surface of the five real band cone filter bank, $\mathbf{d_D} \equiv [1/\sqrt{3} \;\; 1/\sqrt{3} \;\; 1/\sqrt{3}]^{\mathbf{T}}$, $\varepsilon \equiv 20^o$. All frequencies shown in radians.

highly directional case prescribed by $\varepsilon \equiv 5^o$, with all other parameters unaltered from Case 1. It is concluded that the cone-shaped passband may be obtained over a wide range of angles ε, implying the capability to selectively filter ST PWs having DOAs that are prescribed over a range of angles. Small cone angles, having -3-dB contours of less than one degree, may be achieved using this filter bank structure, implying that *a priori* knowledge of the DOA permits excellent attenuation of undesired broad-band signals, such as reflected planes waves having stopband DOAs.

Case 3: Rotation of the Direction of the Cone Axis: The direction of the axis of the cone may be rotated from direction $\mathbf{d_{DO}}$ to a required direction $\mathbf{d_D}$ by means of the rotation matrix $\mathbf{R}$ that satisfies $\mathbf{d_D} = \mathbf{R}\mathbf{d_{DO}}$.

In this case, the required direction of the axis of the cone is off-axis and prescribed by $\mathbf{d_D} \equiv [1/\sqrt{3} \;\; 1/\sqrt{3} \;\; 1/\sqrt{3}]^{\mathbf{T}}$ with $\varepsilon \equiv 20°$. This design specification is similar to Case 1 except that the cone is rotated in $\boldsymbol{\omega}$ by the orthogonal rotation matrix $\mathbf{R}$. Therefore, we rotate the design in Case 1 by solving for $\mathbf{R}$ in

$$[1/\sqrt{3} \quad 1/\sqrt{3} \quad 1/\sqrt{3}]^{\mathbf{T}} = \mathbf{R}[0 \quad 0 \quad 1]^{\mathbf{T}}$$

and simply choosing $\mathbf{d_1} = \mathbf{R}[1 \quad 0 \quad 0]$ and $\mathbf{d_2} = \mathbf{R}[0 \quad 1 \quad 0]$ in equation (5.6) to obtain the corresponding rotated frequency response transfer function $|T_{\mathrm{CONE}}(e^{j\boldsymbol{\omega}})|$. The resultant -3-dB level contour of $|T_{\mathrm{CONE}}(e^{j\boldsymbol{\omega}})|$ is shown (from three different perspectives) in Fig. 7. Note that this design is limited to the half-Nyquist box $|\omega_{1,\,2,\,3}| \leq \pi/2$, corresponding to only 5 real bands, in order to avoid the previously mentioned warping of the 3-D passband that is caused by the bilinear transformation. That is, the upper 4 real bands are omitted in the filter bank.

VII. Verification of Spatio–Temporal Performance

The spatio–temporal performance is described here for the highly-directional Case 2 under broad-band conditions.

A sampled broad-band stochastic *passband* 3-D input PW $x_{\mathrm{PW1}}(n_1, n_2, n_3)$, having direction $\mathbf{d_D} = [0 \quad 0 \quad 1]^{\mathbf{T}}$, and a corresponding stochastic *stopband* 3-D input PW $x_{\mathrm{PW2}}(n_1, n_2, n_3)$, having direction $\mathbf{d_D} = [1/\sqrt{3} \quad 1/\sqrt{3} \quad 1/\sqrt{3}]^{\mathbf{T}}$, are created as described in the Appendix. These PWs have *very broad-band spectra that uniformly cover 80% of the Nyquist spectrum* on the line of their ROS.

The corresponding spatio–temporal output sequences $y_{\mathrm{PW1,\,PW2}}(n_1, n_2, n_3)$ have been computed by deriving the input–output 3-D difference equation from equation (2.1) and separately applying the above signals $x_{\mathrm{PW1,\,PW2}}(n_1, n_2, n_3)$. With the standard deviations $\sigma_{xpw1,\,xpw2}$ of both input PWs $x_{\mathrm{PW1,\,PW2}}(n_1, n_2, n_3)$ scaled to unity, the standard deviations of the corresponding 3-D output signals have been calculated as follows:

$$\sigma_{ypw1} = 0.9204 \quad \text{and} \quad \sigma_{ypw2} = 0.0586 \tag{6.2}$$

over their ROS (of size $64 \times 64 \times 32$). As expected, the standard deviation of the 3-D passband signal is close to unity and that of the stopband signal is much attenuated.

Signal Distortion: In many broad-band applications, distortion of the 3-D passband output signal $y_{\mathrm{PW1}}(n_1, n_2, n_3)$ in the ST-domain, relative to the input signal $x_{\mathrm{PW1}}(n_1, n_2, n_3)$, is an important and sometimes critical consideration. This distortion cannot be determined from the magnitude frequency response and is a strong function of the transient ST-domain response of the 3-D filter. Accordingly, the temporal distortion of the passband PW is defined here as a function of intra-frame distance N from the spatial origin in (n_1, n_2, n_3) as follows:

$$\begin{aligned} d(N, N, n_3) &\\ \equiv y_{\mathrm{PW1}}&(N, N, n_3 - (M+1)/2) - x_{\mathrm{PW1}}(N, N, n_3), \\ N &= 1, 2, 3, \ldots, 64 \end{aligned} \tag{6.3}$$

which must ideally diminish to zero as N increases (that is, as the spatial transient response decays). The final measure of passband temporal distortion $D(N)$ is defined as

$$D(N) = \frac{10}{\sigma_{x\mathrm{pw1}}} \log_{10} \mathrm{stdev}[\{d(N,N,1),\, d(N,N,2),\, \ldots,\, d(N,N,N_3)\}] \tag{6.4}$$

which is the input-normalized distortion power in a line in the temporal direction, *over N_3 frames of the delayed temporal ROS*, at intra-frame horizontal and vertical spatial distances N from the origin in (n_1, n_2, n_3). The function $D(N)$ is shown for this design case as the solid curve in Fig. 8 with $N_3 = 32$ temporal frames and for $N = 8, 9, 10, \ldots, 64$. For $N < 8$, the ST transient response causes unacceptably high distortion implying that 64 spatial sensors are required.

Reduced Input Bandwidth: The asterisked data points in Fig. 8 are the distortion $D(N)$ in the output PW due to an input passband PW for which the bandwidth is reduced from 80% to 40% of the Nyquist interval (corresponding to $k_L \equiv 3\pi/10$, $k_U \equiv 7\pi/10$ in the Appendix). The distortion $D(N)$ is much less in this case primarily because the effects of long spatial transients are reduced as a result of the reduction in low frequency content of the input PW. This case illustrates the relative difficulty of filtering highly *broad-band* PWs having significant low frequency content. In contrast, narrow-band PWs will result in much lower distortion $D(N)$ and require fewer bands and fewer spatial sensors in the cone filter bank.

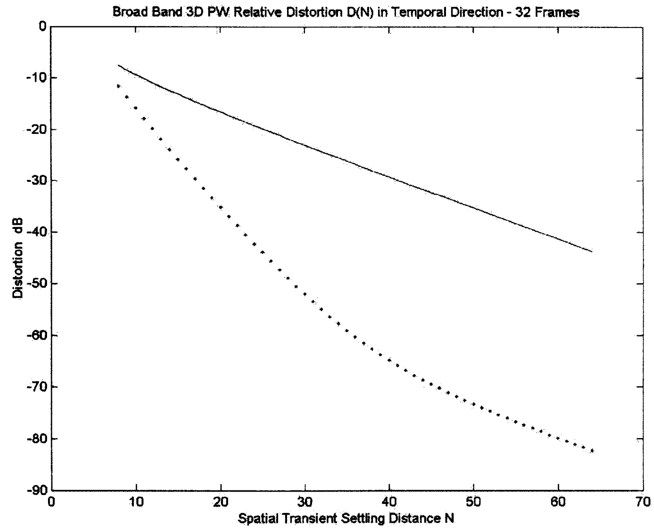

Fig. 8. Distortion $D(N)$ of passband PW versus spatial settling distance N. Solid—80% of Nyquist limit. Asterisks—40% of Nyquist limit.

The above ST-domain data confirm that this 5° 9-band 3-D cone filter bank design case achieves good rejection of broad-band stopband stochastic sampled 3-D PWs while faithfully transmitting a sampled broad-band stochastic passband 3-D PW that has similar spectral distribution and signal power (prior to sampling).

VIII. Summary

A 3-D cone filter bank is proposed that employs band limited uniform bandwidth 3-D filters in each band having band limited beam-shaped passbands. It is shown that this 3-D cone filter bank yields algebraic expressions for the steady-state frequency response in the 3-D discrete-domain. Further, it has been demonstrated, by means of the 3-D discrete-domain implementation in the ST domain, that the 3-D cone filter bank transmits broad-band passband PWs with low attenuation and low distortion while significantly attenuating broad-band stopband PWs. In the ROS of the 3-D ST output signal where the output transient response has effectively decayed, the filter bank achieves almost exact delayed-PR of passband PWs.

The proposed 3-D cone filter bank may be improved upon in a number of ways. First, it is well known that polyphase structures provide an efficient way of implementing the filter bank in equation (5.3) and that multi-rate polyphase implementations permit *full temporal decimation* by N of each band, in the direction n_3. The polyphase method leads to a significant reduction in the computational complexity of the individual bands of the 3-D cone filter bank. Full decimation of each band by N implies that the quantity of data is approximately the same as that employed in a single 3-D beam filter [5]. In such a full decimation process, *each real band* is implemented by first employing a conventional analysis filter (such as the N-band filters used here) prior to temporal down sampling by N, followed by 3-D beam filtering of the down sampled data, followed by up sampling by N prior to conventional synthesis filtering. Temporal wavelet filters are obvious alternative candidates to N-band filters for the analysis and synthesis sections.

The functions $H_{\mathrm{FP1,\,FP2}}(\mathbf{s})$ in equation (3.1) may be replaced by narrow *band-stop* filters of the form $\mathbf{d}_{\mathbf{1,\,2}}^{\mathbf{T}}\mathbf{s}/(B_{1,\,2} + \mathbf{d}_{\mathbf{1,\,2}}^{\mathbf{T}}\mathbf{s})$ to realize a new 3-D-*Stop* cone filter bank having a highly directional 3-D cone-shaped *stop* passband that may be used to *selectively attenuate* (that is, jam) a broad-band ST 3-D PW on the basis of its DOA. Such filters are the subject of further investigation.

Highly directional 3-D cone filter banks (and the above-mentioned 3-D-Stop cone filter banks) may be used for the selective filtering of PWs on the basis of their DOAs under stringent conditions. For example, a combination of cone-pass and cone-stop 3-D filter banks could selectively enhance a desired broad-band 3-D PW while selectively attenuating (i.e., jamming) a number of broad-band PWs on the basis of their DOAs. It is conjectured that such filter banks may be used to recover a broad-band target PW on the basis of its DOA under fading conditions due to multipath cancellations.

It is well known that the number of sensors in beamforming linear arrays may be reduced, relative to equivalent linear shift invariant beamforming arrays, by employing adaptive filtering techniques. Similarly, adaptive versions of 3-D cone filter banks should also be useful for reducing the complexity of the filter bank and for adapting to the time-varying nature of the received signals. The existence of the algebraic expression for the 3-D frequency response suggests that the potential exists to adapt the direction $\mathbf{d_D}$ and angle ε, as functions of time, in 3-D tracking applications where a PW from a moving far-field source could be tracked over time. Further, adjustable weights could be introduced into each band of the filter bank, allowing the shape of the cone to be adapted over time in a way that improves the enhancement of PWs in the presence of stopband signals.

As in conventional beamforming applications, the potential exists to reduce the complexity of such filter banks by adapting the coefficients of the filter bank in order to reduce the number of spatial sensors.

There are a number of ways in which, if necessary, the level contours of the steady-state magnitude frequency-response could be made to more closely approximate the circular cross section of an ideal cone. First, the level contours, in planes perpendicular to the axis of the cone, can be brought in to *closer proximity to a circle* by using four or six beam filters in each band k instead of two as reported here, arranged in such a way as to possess quadrantal or hexagonal symmetry, respectively, when viewed along the center line CL of the cone. Second, much *sharper cone transition bands* are possible by choosing higher order prototype functions in equation (3.1) for the frequency-planar filters $H_{\mathrm{FP1,2}}(\mathbf{s})$. However, it is a consequence of employing higher order filters that the size of the input and output masks must be larger, implying increased complexity. Also, narrower bandwidths may lead to undesirable longer spatial transients at the computational starting edges of the 3-D output image.

Finally, the potential exists to significantly reduce the number of required spatial samples (and therefore sensors) by reducing the transient settling time. This might be accomplished in a number of ways. One approach is to adaptively determine nonzero initial conditions at the edges of the 3-D input mask, designed to achieve short settling transient distances.

APPENDIX
PASSBAND AND STOPBAND SAMPLED BROAD-BAND PWs

Spatio–temporal performance has been confirmed by constructing two sampled broad-band 3-D input PWs. Both PWs are obtained by sampling zero mean band limited 1-D random sequences.

A stochastic sequence $x(n_3) = rand(-(1/2),\, 1/2)$, $n_3 = 0,\, 1,\, 2,\, \ldots,\, 127$ consists of a sequence of 128 randomly distributed real numbers on the closed interval $[1/2 \;\; -1/2]$ having DFT $X(k)$, $k = -63$ to 64. This sequence is then band limited to approximately 80% of the Nyquist spectrum using the window function

$$W(k) \equiv \begin{matrix} 1, & \lfloor 128k_L \rfloor \le |k| \le \lfloor k_U 128 \rfloor \\ 0, & \text{otherwise} \end{matrix}$$
$$k_L = 1/10,\; k_U = 9/10$$

yielding a 1-D *band limited* stochastic broad-band 1-D sequence

$$x_{\mathrm{RANDOM1}}(n_3) = \mathrm{IDFT[X(k)W(k)]}$$

and the corresponding 3-D sampled broad-band stochastic *passband* PW

$$x_{\mathrm{PW1}}(n_1,\, n_2,\, n_3) = x_{\mathrm{RANDOM1}}(n_3). \tag{6.5}$$

A sampled version of a the 3-D *stopband* PW, having direction $\mathbf{d_D} \equiv [1/\sqrt{3},\, 1/\sqrt{3},\, 1/\sqrt{3}]^{\mathbf{T}}$, is created by selecting

$$x_{\mathrm{PW2}}(n_1,\, n_2,\, n_3) = x_{\mathrm{RANDOM2}}(n_1 + n_2 + n_3) \tag{6.6}$$

where $x_{\mathrm{RANDOM2}}(n_3) = \mathrm{IDFT[X(k)W(k)]}$ with $k_L = 1/10\sqrt{3}$ and $k_U = 9/10\sqrt{3}$. This choice of $k_{U,\,L}$ ensures that the *continuous-domain* band limited PWs, corresponding to the discrete-domain PW equations (6.5) and (6.6), have equal broad bandwidths equal to 80% of the Nyquist temporal frequency interval $0 \le \omega_3 \le \pi$.

ACKNOWLEDGMENT

The author gratefully acknowledges the suggestions of the anonymous reviewers.

REFERENCES

[1] L. T. Bruton and N. R. Bartley, "Highly selective three-dimensional recursive beam filters using intersecting resonant planes," *IEEE Trans. Circuits Syst.*, vol. CAS-30, pp. 190–193, Mar. 1983.

[2] ——, “The design of highly selective adaptive three-dimensional recursive cone filters,” *IEEE Trans. Circuits Syst.*, vol. CAS-34, pp. 775–781, July 1987.

[3] P. Agathoklis and L. T. Bruton, “Practical BIBO-stability of n-dimensional discrete systems,” *Proc. Inst. Elect. Eng.*, pt. G, vol. 130, no. 6, 1983.

[4] G. Runze and P. Steffen, “A contribution to the design of three-dimensional digital FIR and IIR cone-filters,” in *Proc. 3-D Image Analysis and Synthesis*, Nov. 1996.

[5] G. Runze, “Efficient design of digital 3-D cone-shaped FIR fan-filters using transformation,” in *Proc. 10th IEEE Workshop on Image and Multidimensional Signal Processing 1998, (IMDSP Workshop 98)*, Alpbach, Austria, July 1998, pp. 263–266.

[6] ——, “Efficient implementation of digital 3-D IIR filters for separation of velocity components in data-streams,” in *Proc. 2nd IMACS International Conf. Circuits, Systems Computers (IMACS-CSC’98)*, Piraeus, Greece, 1998, pp. 631–634.

[7] P. P. Vaidyanathan, *Multirate Systems and Filter Banks*. Englewood Cliffs, NJ: Prentice-Hall, 1993, ch. 8.

[8] L. T. Bruton, “Selective filtering of spatio–temporal plane waves using 3-D cone filter banks,” in *Proc. 2001 IEEE Pacific Rim Conf. Communications and Signal Processing (PACRIM 2001)*, Victoria, BC, Canada, Aug. 26–28, 2001, pp. 67–70.

[9] D. M. Goodman, “Some difficulties with double bilinear transformation in 2-D recursive filter design,” *Proc. IEEE*, vol. 66, pp. 796–797, July 1978.

[10] ——, “Some stability properties of two-dimensional linear shift-invariant digital filters,” *IEEE Trans. Circuits Syst.*, vol. CAS-24, pp. 201–208, Apr. 1977.

L. T. Bruton (M’71-M’80–F’81) is a Professor of Electrical and Computer Engineering at the University of Calgary, Calgary, AB, Canada, where he carries out research in the fields of analog and digital signal processing with emphasis on multidimensional (MD) circuits and systems applied to the design and implementation of 2-D, 3-D, and 4-D image enhancement using MD filtering techniques, on MD filter banks, on the tracking of 3D objects and on data hiding in 2-D and 3-D signals. He is especially interested in the applications of 2-D and 3-D filters for practical purposes in such fields as video processing, seismic, and audio signal processing. He is the inventor of a number of widely used filtering methods, including the class of frequency-dependent negative resistance (FDNR) analog filters, and the class of lossless discrete integrator (LDI) discrete-domain filters.

Dr. Bruton is the recipient of the 2002 Education Award of the IEEE Circuits and Systems Society, the 50th Jubilee Medal of the IEEE Circuits and Systems Society, the 1994 Outstanding Engineer Award of IEEE Canada (Region 7) "for leadership in engineering and the engineering profession and for research in the field of microelectronic digital and analog real-time filter design,” the 1992 Manning Principal Award for Innovation, Canada, the 1992 Alberta Science and Technology Award (ASTech) for Innovation in Science “in recognition of his leadership in science,” and the 1993 Federal Government of Canada’s 125th Anniversary of Canadian Confederation Medal “in recognition of his significant contributions to compatriots, community and to Canada.” He is one of 162 scientists selected for inclusion in the textbook *Great Canadian Scientists* (Barry Shell, Vancouver, BC, Canada: Polestar, 1997), and is a Member of the Royal Society of Canada